PERGAMON

International Journal of Heat and Mass Transfer 42 (1999) 3757–3770

International Journal of HEAT and MASS TRANSFER

www.elsevier.com/locate/ijhmt

Heat/mass transfer characteristics in two-pass smooth channels with a sharp 180-deg turn

M. Hirota[a,*], H. Fujita[a], A. Syuhada[a], S. Araki[b], T. Yoshida[c], T. Tanaka[d]

[a]*Department of Mechanical Engineering, Nagoya University, Chikusa-ku, Nagoya 464-8603, Japan*
[b]*Suzuki Co. Ltd., Takatsuka, Hamamatsu 432-8065, Japan*
[c]*Department of Environmental Science and Technology, Shinshu University, Wakasato, Nagano 380-8553, Japan*
[d]*Electric Power R&D Center, Chubu Electric Power Co., Inc., Odaka, Midori-ku, Nagoya 459-8001, Japan*

Received 27 July 1998; received in revised form 1 February 1999

Abstract

Heat/mass transfer characteristics for turbulent flow in rectangular cross-sectioned two-pass channels with a sharp 180-degree turn have been examined experimentally using the naphthalene sublimation method. The channel cross-section is 50×25 mm, and three turn clearances of 30, 50, and 70 mm have been tested under Reynolds numbers of $(2.0–6.0) \times 10^4$. Local mass transfer rates on all walls of the channel have been measured to clarify the three-dimensional heat and fluid flow characteristics in the channel. Detailed maps of the local Sherwood number are presented, which make clear the complex and steep changes in the local heat/mass transfer rates in and after the sharp turn section and their dependency on the turn clearance and Reynolds number.

1. Introduction

Rectangular cross-sectioned channels with sharp 180-degree turns are often utilized for the passage of fluids in various types of thermal equipment. One of the typical applications is found in the internal cooling passages of gas turbine components exposed to high-temperature gas flow [1–15]. The flow field in those channels has a three-dimensional structure due to the additive effects of the secondary flow induced by the centrifugal force in flowing around the turn [16] and the flow separation caused by the abrupt change in the flow direction in the turn [1]. Therefore, under forced convection heat transfer, the local heat transfer rates are expected to change steeply in a complex manner. Since steep variations in the local heat transfer rates increase the thermal stresses and affect the lifetime of the components, detailed data on the local heat transfer in those channels are indispensable for the design of components used under severe thermal conditions.

Concerning the rectangular channels with 'mild' 180° turns of large curvature, i.e., U-bends, a number of research studies have been conducted on fluid flow and forced-convection heat transfer [17–21]. The flow structure and local heat transfer characteristics in the channel with the 'sharp' 180° turns are, however, much more complicated than those in the U-bends due to the flow separation and reattachment around the turn, and thus the results obtained in U-bends cannot be applied directly to channels with sharp 180° turns. Hence, several studies have been conducted to date on forced convection heat/mass transfer in rectangular channels with sharp 180° turns under stationary [2–4] and rotating conditions [5–8]. Those pioneer studies contributed much to the understanding of overall or

* Corresponding author. Fax: +81-52-789-2703.

0017-9310/99/$ - see front matter
PII: S0017-9310(99)00057-5

Nomenclature

C	turn clearance
D	naphthalene–air molecular diffusion coefficient
d_h	hydraulic diameter of the channel
h_m	local mass transfer coefficient
K	coefficient of pressure loss, defined by Eq. (1)
P	local pressure
P_a	atmospheric pressure
Re	Reynolds number $= U \times d_h/\nu$
Sh	local Sherwood number $= h_m \times d_h/D$
Sh_B	block-averaged Sherwood number, defined by Eq. (4)
Sh_m	mean Sherwood number averaged over whole test section
Sh_{md}	Sherwood number averaged in the downstream half of the test section
Sh_{mu}	Sherwood number averaged in the upstream half of the test section
U	bulk velocity of air

Greek symbols

ρ_a	density of air
ν	viscosity of air

semi-local characteristics of the heat/mass transfer in the channel.

In general, however, detailed measurements or numerical predictions of local heat transfer rates in channels with sharp turns are very difficult even in the stationary condition because of the complexities in channel geometry. Therefore, few reports have been available on local heat/mass transfer characteristics in the channel. Besserman and Tanrikut [9], Wang et al. [10], Astarita et al. [11], and Hirota et al. [12] presented contour maps of local Nusselt or Sherwood numbers on the channel wall. The contour mapping of the results was an intuitively clear way to present the complex distribution of local heat transfer rates on the channel wall; however, since those results were limited to the distribution on only one principal wall of the channel, they were not enough to clarify the three-dimensional characteristics of local heat transfer inherent to the rectangular channel with sharp turns. On the other hand, Han and his coworkers [13,14] and Murata et al. [15] measured the local heat/mass transfer rates on all walls of the channel. They revealed that, due to the three-dimensional flow field in the channel, the local heat/mass transfer characteristics on one channel wall are considerably different from those on the other walls, but the density of the measuring points in their experiments were not so high as to enable them to present the contour maps of the local Nusselt numbers.

For a better understanding of the forced convection heat transfer in a rectangular channel with sharp 180° turns, it is desirable to measure the local heat transfer rates on all walls of the channel at a high data density and to present the results in the form of contour maps. Moreover, detailed experimental data obtained on all channel walls provide a better database for an evaluation of the results of computer simulation as well as for the design of high-temperature components. With these points as background, we have conducted an experimental study to make clear the detailed local heat/mass transfer characteristics over all the walls of rectangular channels with a sharp 180° turn under the stationary condition. Three turn clearances have been tested under the Reynolds-number range of turbulent flow (2.0–6.0) $\times$ 10^4. The naphthalene sublimation method has been used to measure the local heat/mass transfer rates with a sufficiently high spatial resolution and a high density of measuring points [22]. We have also measured the local pressure distributions in the channel to estimate the characteristics of the flow field. The distributions of local Sherwood numbers on all channel walls are presented in the form of contour maps, and influences of the turn clearance and

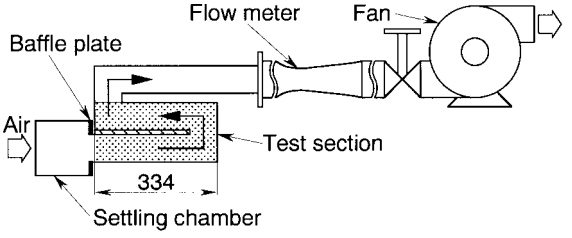

Fig. 1. Schematic diagram of the experimental apparatus.

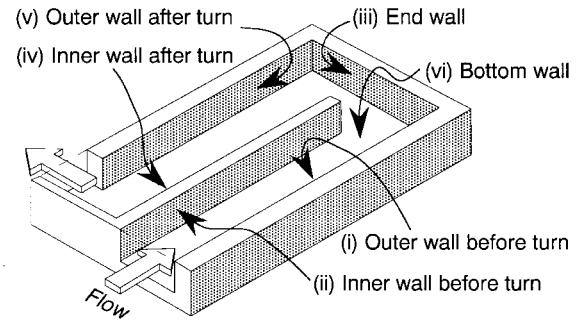

Fig. 2. Test section.

Reynolds number on local heat/mass transfer are examined in detail.

2. Experiments

Fig. 1 shows a schematic diagram of the experimental apparatus. Since the naphthalene sublimation method was used to measure the local mass transfer rate, the apparatus was operated in a suction mode to exclude a rise in temperature of air caused by a turbofan. Air flows into the test channel through a settling chamber in which the entrance condition of the inlet air flow is set up. As shown in detail later, a baffle plate is equipped at the entrance of the test channel. The test channel has a rectangular cross-section of 50 $\times$ 25 mm (hydraulic diameter $d_h = 33.3$ mm), and has two sharp 180° turns. The mass transfer rates and pressure distributions were measured in the darkened region of the figure, which includes the first turn section and is positioned just downstream of the settling

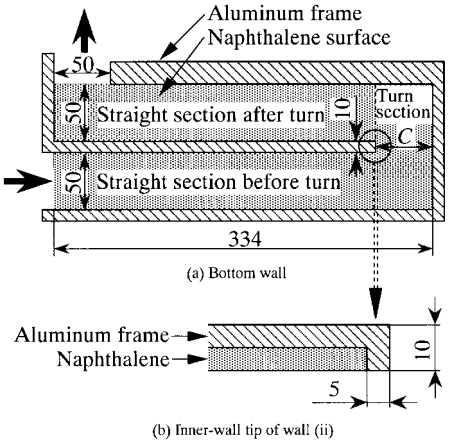

Fig. 3. Details of the bottom wall and near the inner-wall tip. (a) Bottom wall; (b) inner-wall tip of wall (ii).

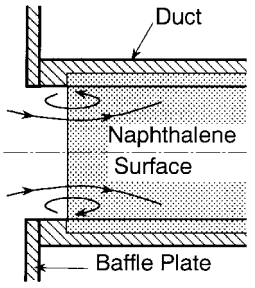

Fig. 4. Configuration of the channel entrance.

chamber. Air contaminated by the naphthalene vapor is then exhausted from the building by a turbofan.

Fig. 2 shows a schematic illustration of the test section, i.e., the darkened region of Fig. 1. In this study, we measured the local mass transfer rates over all the channel walls shown in Fig. 2, namely, (i) outer wall before the turn; (ii) inner wall before the turn; (iii) end wall; (iv) inner wall after the turn; (v) outer wall after the turn; (vi) bottom wall (or top wall). The outer, inner, and end walls are the short-side walls (25 mm width), and the bottom and top walls are the long-side walls (50 mm width). We confirmed that the results obtained on the top wall agreed well with those on the bottom wall, qualitatively and quantitatively; thus, for the long-side walls, it suffices to show the results on the bottom wall only. The details of the bottom wall in the test section are shown in Fig. 3(a); the dark region corresponds to the naphthalene surface, and the hatched region is the aluminum frame that supports the naphthalene surface. The partition (inner) wall which divides the naphthalene surface into two straight sections before and after the turn is 10 mm thick. By changing the length of this wall, the turn clearance ('C' in Fig. 3(a)) can be set at 30, 50 or 70 mm. The distance between the channel entrance and the inner-wall tip changes in the range from 264 mm ($=7.93d_h$) to 304 mm ($=9.13d_h$) depending on the turn clearance. Fig. 3(b) is a close-up of the inner-wall tip. The inner-wall tip has a square configuration and is made of aluminum frame; thus, the regions up to 5 mm from the inner-wall tip on walls (ii) and (iv) are inactive in mass transfer.

Fig. 4 shows the details of the entrance configuration of the channel. A baffle plate was placed at the entrance of the test channel to form a sharp-edged entrance, which ensured that the air flow entering the test section had an abrupt contraction-entrance condition with strong turbulence [23]. This flow-inlet condition was selected rather arbitrarily to simulate the channels used in compact heat exchangers which have a wide range of flow-inlet conditions [24]. Here, it should be noted that, in conducting the mass transfer experiment, only the wall on which the local mass

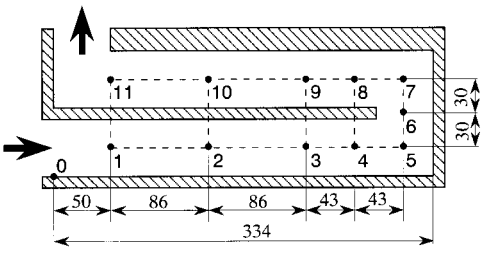

Fig. 5. Locations of pressure taps.

transfer rates were measured had a naphthalene surface, while other walls were made of aluminum plates. Since no concentration boundary layers exist on the aluminum walls, the values of local Sherwood numbers measured under this situation may be somewhat different from those obtained under the condition in which all wall surfaces are coated by naphthalene. It is, however, thought that such differences in local Sherwood numbers are rather small, because the turbulent mixing is so strong in the present flow condition that the naphthalene vapor is expected to have a uniform concentration profile in a cross-section in the present experimental setup.

The local mass transfer coefficient h_m was calculated from the difference in the naphthalene surface profiles before and after each data run, which were measured by a digital linear gage with an accuracy of 1 μm. It was passed over the naphthalene surface by a computer-controlled two-dimensional positioner at a 0.2 mm pitch in the streamwise direction and at a 2.5 mm pitch (long-side wall) or 1.25 mm pitch (short-side wall) in the spanwise direction. In each data run, the naphthalene surface was exposed to the air flow for 1–1.5 h, so that the maximum sublimation depth of the naphthalene surface was less than 0.2 mm.

The pressure distribution was also measured to estimate the qualitative characteristics of the flow field. The locations of the pressure taps are shown in Fig. 5. Twelve pressure taps were distributed in the test section; one pressure tap was on the outer wall near the channel entrance, and eleven taps were on the spanwise centerline of the bottom wall. In addition to the three turn clearances mentioned above, the pressure distributions were measured for two more turn clearances of $C=40$ and 60 mm. The mass transfer experiments and pressure measurements were conducted under the Reynolds number Re of $(2.0–6.0)\times10^4$, which corresponds to the turbulent flow condition.

3. Results and discussion

3.1. Pressure distribution

Fig. 6 shows the distributions of the dimensionless

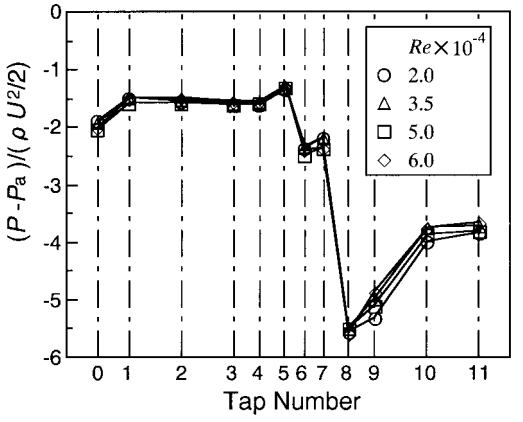

Fig. 6. Pressure distributions for different Re ($C=50$ mm).

pressure obtained in the channel with a medium turn clearance $C=50$ mm for various Re. The abscissa shows the pressure-tap number defined in Fig. 5, and the ordinate shows the dimensionless differential pressure. The flow characteristics in the channel can be estimated qualitatively as follows.

The pressure shows the local minimum at the pressure tap numbered 0 (denoted as Tap 0) that is located near the channel entrance, which then increases once at Tap 1 and decreases monotonously in the flow direction up to Tap 4. This shows that the flow is separated at the edge of the baffle plate, and that the separated flow reattaches on the channel walls causing the pressure recovery at Tap 1, with the resulting pressure loss caused by the wall friction after Tap 1. At Tap 5, located in the upstream half of the turn section, the pressure slightly increases; this pressure rise is caused by the impingement of the flow, which enters the turn section through the straight section, against the end wall (wall (iii) in Fig. 2). After the pressure reaches its

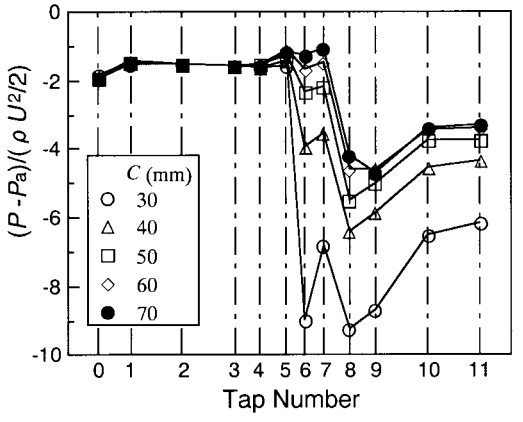

Fig. 7. Pressure distributions for different C ($Re=3.5\times10^4$).

local minimum at Tap 6, it increases once at Tap 7 and then decreases very steeply to attain the minimum at Tap 8. This complex change in pressure distribution suggests that the flow is separated at the tip of the inner wall and that a separation bubble is formed in the straight section after the turn. The pressure rise observed at Tap 7 is attributed to the impingement of the flow passing through the turn clearance against the outer wall (wall (v) in Fig. 2); this mechanism of pressure rise is similar to that encountered at Tap 5. The pressure recovers after the separation bubble, and it approaches an asymptotic value at Tap 11.

Fig. 7 shows a comparison of the dimensionless pressure distributions obtained for different turn clearances at a constant Re of 3.5×10^4. The pressure at Tap 6 diminishes as the turn clearance is decreased, because the decrease in the turn clearance causes an acceleration of the flow passing through it. The difference in the pressures at Taps 6 and 8 becomes smaller with the decrease in the turn clearance, whereas the pressure difference between Taps 7 and 8 is almost constant irrespective of the turn clearance except for the case of $C=30$ mm. It can be estimated that the flow structure after the turn for $C=30$ mm has some unique characteristics which are different from those for larger turn clearances.

3.2. Coefficient of pressure loss

Based on the pressure distributions shown above, the coefficient of pressure loss K, which is defined by the following equation, was calculated.

$$K = \frac{2 \times (P_0 - P_{11})}{\rho_a U^2} \tag{1}$$

P_0 denotes the static pressure at the channel entrance, and P_{11} is that measured at Tap 11 located near the exit of the test section. Since P_0 could not be measured directly in the present channel due to the flow separation at the channel entrance, it was obtained by applying Bernoulli's equation to the flow far from the channel entrance and that at the channel entrance; the former is stationary and in the atmospheric pressure P_a. Assuming that the flow velocity at the channel entrance is equal to the bulk air velocity U, P_0 is given by the following equation.

$$P_0 = P_a - \frac{\rho_a U^2}{2} \tag{2}$$

Consequently, K is expressed as follows.

$$K = \frac{2 \times (P_a - P_{11})}{\rho_a U^2} - 1 \tag{3}$$

Fig. 8 shows the variations of K against Re. K is nearly constant against Re, and C is decisive for K-values. The values of K generally increase as the turn clearance is decreased, and those for $C=30$ mm are significantly larger than those for wider turn clearances. The solid symbols in the figure show the results obtained by Metzger et al. [1] in the channel which is equivalent to that of $C=50$ mm in the present experiment. The present results of K for $C=50$ mm agree well with their results.

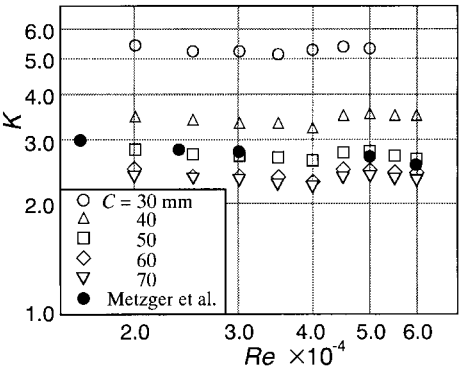

Fig. 8. Coefficients of pressure loss.

3.3. Mean Sherwood number

The Sherwood number averaged over the whole naphthalene surface in the test section, denoted as Sh_m, was calculated from the total amount of naphthalene sublimated during the data run. Fig. 9 shows the Sh_m distributions vs Re obtained for $C=50$ mm. In addition to Sh_m, the Sherwood numbers averaged in the upstream half and downstream half of the test section, denoted as Sh_{mu} and Sh_{md}, respectively, are also shown. Sh_m, Sh_{mu}, and Sh_{md} increase exponentially with Re. The values of Sh_{md} are 1.3–1.4 times as large as those of Sh_{mu}; this means that the mass-transfer-

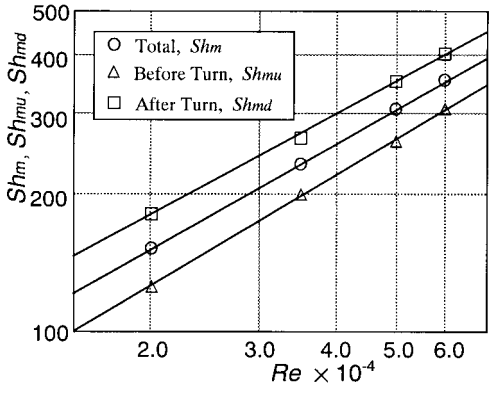

Fig. 9. Mean Sherwood numbers ($C=50$ mm).

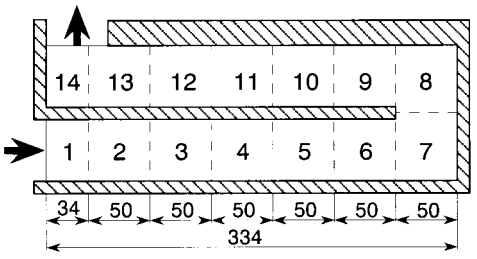

Fig. 10. Definition of blocks ($C=50$ mm).

enhancement effect of the sharp turn is greater than that of the sharp-edged entrance. Qualitatively similar results have been obtained in other test channels with different turn clearances. From a quantitative viewpoint, the values of Sh_m, Sh_{mu}, and Sh_{md} in the channel of $C=70$ mm were almost the same as those for $C=50$ mm; while Sh_m and Sh_{md} for $C=30$ mm were 1.2 times and 1.3 times as large as those for $C=50$ mm, respectively.

3.4. Block-averaged Sherwood number

In order to obtain an overall view of the local mass transfer characteristics in the channel, we divided the test section into 14 blocks as shown in Fig. 10 and calculated the integral-average of the local Sherwood number in each block on each channel wall. This block-averaged Sherwood number, Sh_B, is thus defined by the following equation,

$$Sh_B = \frac{1}{\Delta S}\int\int_{\Delta S} Sh\,dS \tag{4}$$

where ΔS denotes the surface area of each block. Here it should be noted that this definition of Sh_B is not so usual in the case of heat transfer experiment such as stainless-foil heating, in which block-averaged Nusselt number is obtained from the difference of the bulk temperatures of air flow before and after the block. The definition of Eq. (4) was used here because the direct measurement of the bulk-concentration differ-

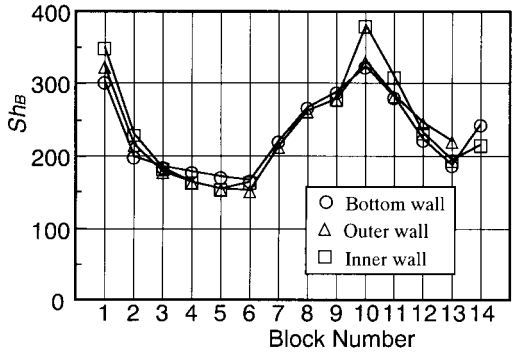

Fig. 11. Block-averaged Sherwood numbers on each channel wall ($C=50$ mm).

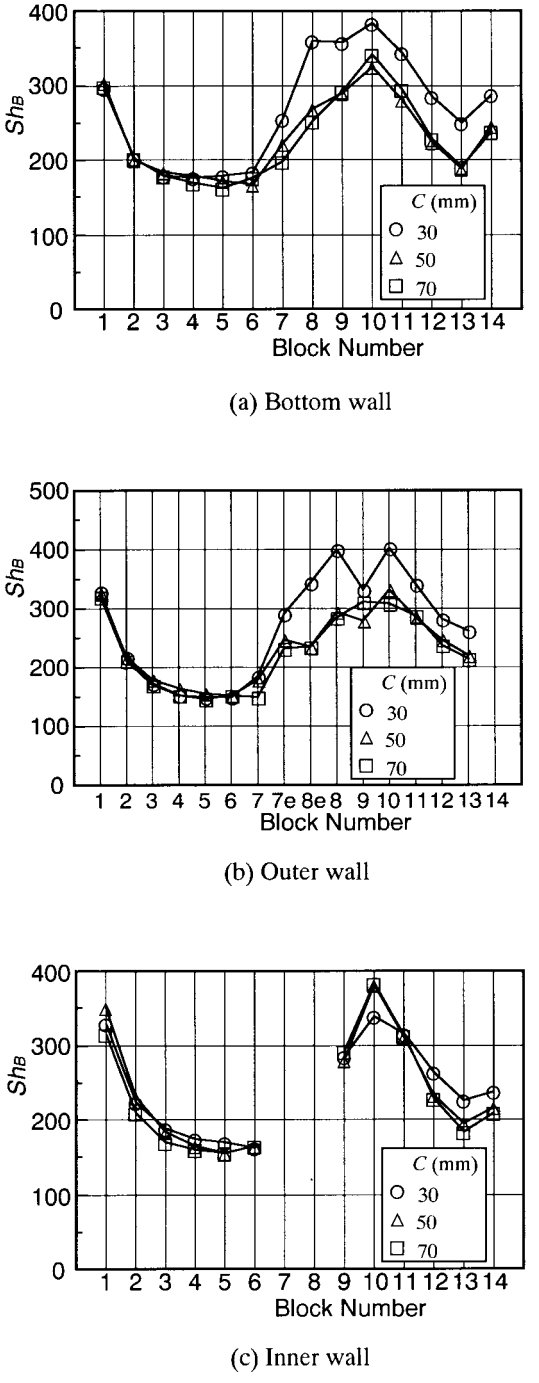

Fig. 12. Block-averaged Sherwood numbers for different C. ($Re=3.5\times10^4$). (a) Bottom wall; (b) outer wall; (c) inner wall.

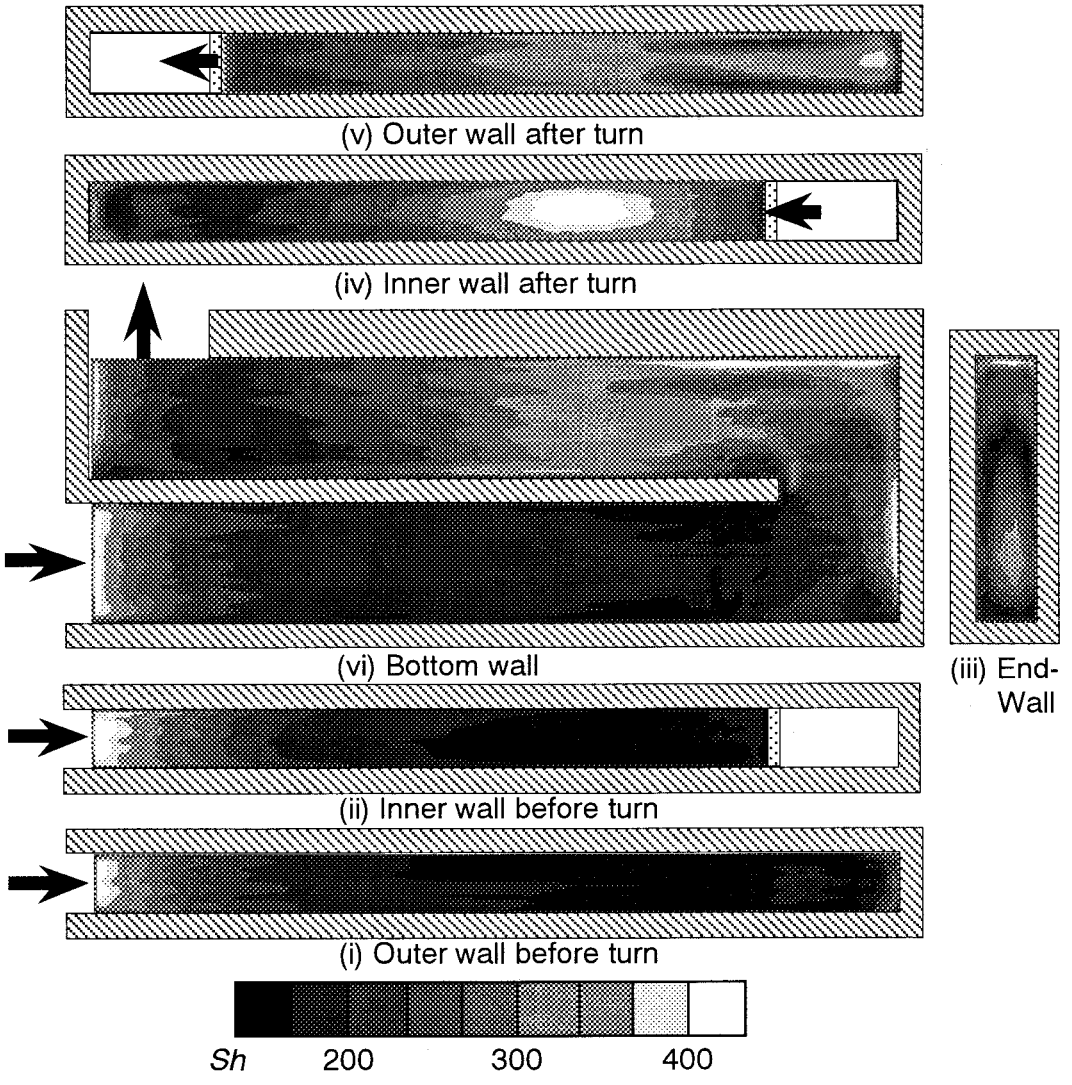

Fig. 13. Local Sherwood number distribution ($C = 50$ mm, $Re = 3.5 \times 10^4$).

ence before and after the block was impossible in the present experimental setup with the naphthalene sublimation method. In this method, the wall boundary condition corresponds to the constant-wall-temperature heating in heat transfer experiment, and thus the values of Sh_B calculated by Eq. (4) agree with those obtained from the bulk-temperature difference.

Fig. 11 shows the typical streamwise variations in Sh_B obtained on each channel wall for $C = 50$ mm and $Re = 3.5 \times 10^4$. The abscissa shows the block-numbers defined in Fig. 10. As a general trend, the distributions of Sh_B on the bottom wall agree well with those on the outer and inner walls, qualitatively and quantitatively. Thus it follows that, for the purpose of grasping the outline of the Sh_B distributions, it is enough to measure the mass transfer rates on either the long-side wall or the short-side walls.

Sh_B shows the maximum in Block 1 located at the entrance of the test section, then decreases in the flow direction because of the development of the concentration boundary layer and reaches minimum in Block 6. Sh_B then increases in the turn section, i.e., Blocks 7 and 8, and attains its local maximum in Block 10 which is located one block downstream of the turn exit. This location of the local maximum Sh_B agrees well with that reported by Chyu [4]. It should be noted that, although the values of Sh_B in Block 10 are almost the same as those in Block 1, Sh_B-values in Block 11 are much larger than those in Block 2. This suggests that the mass-transfer-enhancement effect of the sharp

turn is maintained over a longer distance after the turn than the effect of the abrupt-contracted flow inlet is maintained after the channel entrance. This difference in effective length is reflected in the difference between Sh_{mu} and Sh_{md} observed in Fig. 9. In block 10, Sh_B on the inner wall is larger than that on the other walls; as described in detail later, this high mass transfer rate is caused by the reattachment of the flow, which is separated at the inner-wall tip, on the inner wall. Sh_B increases again in Block 14 due to the influence of the second sharp turn located at the end of the test section.

Figs. 12(a), (b), and (c) shows the Sh_B distributions on the bottom wall, outer wall, and inner wall of the channel, respectively, obtained for different turn clearances. In Fig. 12(b), Blocks 7 and 8 are located on the outer walls (i) and (v) (see Fig. 2), respectively, and Blocks 7e and 8e are on the end wall (iii). As a whole, the values of Sh_B for $C=50$ mm are nearly equal to those for $C=70$ mm on all walls. On the bottom and outer walls, Sh_B-values for $C=30$ mm are notably larger than those for the other channels after Block 7 (Fig. 12(a)) and Block 7e (Fig. 12(b)). However, on the inner wall shown in Fig. 12(c), the influence of C on Sh_B-values is less pronounced than that observed in Fig. 12(a) and (b). On the bottom and inner walls, similarly to Fig. 11, the local maximum of Sh_B appears in Block 10 irrespective of the turn clearance. However, on the outer wall for $C=30$ mm, the local maximum of Sh_B appears in Block 8 as well as Block 10.

3.5. Local Sherwood number

Fig. 13 shows the typical distributions of the local Sherwood number Sh which were obtained under the experimental condition of $C=50$ mm and $Re=3.5\times10^4$. The figure consists of six maps, (i) to (vi), showing the Sh distributions obtained on each channel wall illustrated in Fig. 2. The variations in Sh-values are shown as contrasting light and dark areas of various shading; the maps become whiter as Sh-values increase, and the regions of $Sh>400$ are shown in white. The arrows present the flow directions at the entrance or exit of each section. The characteristics of Sh distributions are described in detail by dividing the test channel into the following three sections; (1) straight section before the turn (Blocks 1–6), (2) turn section (Blocks 7 and 8), and (3) straight section after the turn (Blocks 9–14).

3.5.1. Straight section before the turn

At the entrance of the channel, Sh shows the local maximum on both the short-side and long-side walls; these large mass transfer rates are caused by the strong turbulence produced at the sharp-edged entrance and by the leading-edge effect of the boundary layer. Sh then decreases gradually in the flow direction due to the development of the concentration boundary layer on each channel wall. Sh distributions on the bottom wall agree well with those on the outer and inner walls, qualitatively and quantitatively.

3.5.2. Turn section

At first, Sh distributions in the upstream half of the turn section, i.e., Block 7, are examined in detail. On the bottom wall shown in Fig. 13 (vi), Sh increases gradually in the flow direction, then rises very steeply to attain its local maximum near the junction with the end wall. The relatively gradual increase in Sh mentioned in the former is caused by the secondary flow, which transports fresh air from the core region with low naphthalene-vapor concentration to the vicinity of the bottom wall. On the end wall shown in Fig. 13 (iii), Sh attains the local maximum near the center of Block 7e; this high Sh region is brought about by the impingement of the flow that enters the turn section through the straight section before the turn. The impinging flow is then forced to change its direction by the end wall, and impinges again on the bottom wall. This 'secondary' flow-impingement causes the local maximum of Sh on the bottom wall described above. On the other hand, in the corner of the bottom wall and the end wall, there appears a region of low Sh-values. This suggests that, near the corner in the upstream half of the turn section, the flow separation occurs due to the abrupt change in the flow direction at the sharp turn, resulting in the formation of a recirculation zone of low mass transfer rates [1,15].

In the downstream half of the turn section, i.e., Block 8, the values of Sh on the bottom wall are larger than those in Block 7. This enhancement of mass transfer is caused by an increase in the primary flow velocity, which occurs due to the flow separation at the inner-wall tip and a resulting decrease in the substantial cross-sectional area of the flow passage. This accelerated flow passing through the turn clearance then impinges on the outer wall after the turn, wall (v) in Fig. 2, and thus Sh attains its local maximum near the upstream edge of this wall. Similarly to the case of Block 7, this flow impinging on the outer wall then impinges again on the bottom wall, and thus Sh in Block 8 on the bottom wall shows quite large values along the junctions with the outer wall. On the end wall, Sh decreases once in the flow direction after its local maximum in Block 7e, but increases again to its local maximum near the downstream edge of the wall. This suggests that the above-mentioned flow impinging on the outer wall is then reversed toward the end wall and enhances the mass transfer in Block 8e.

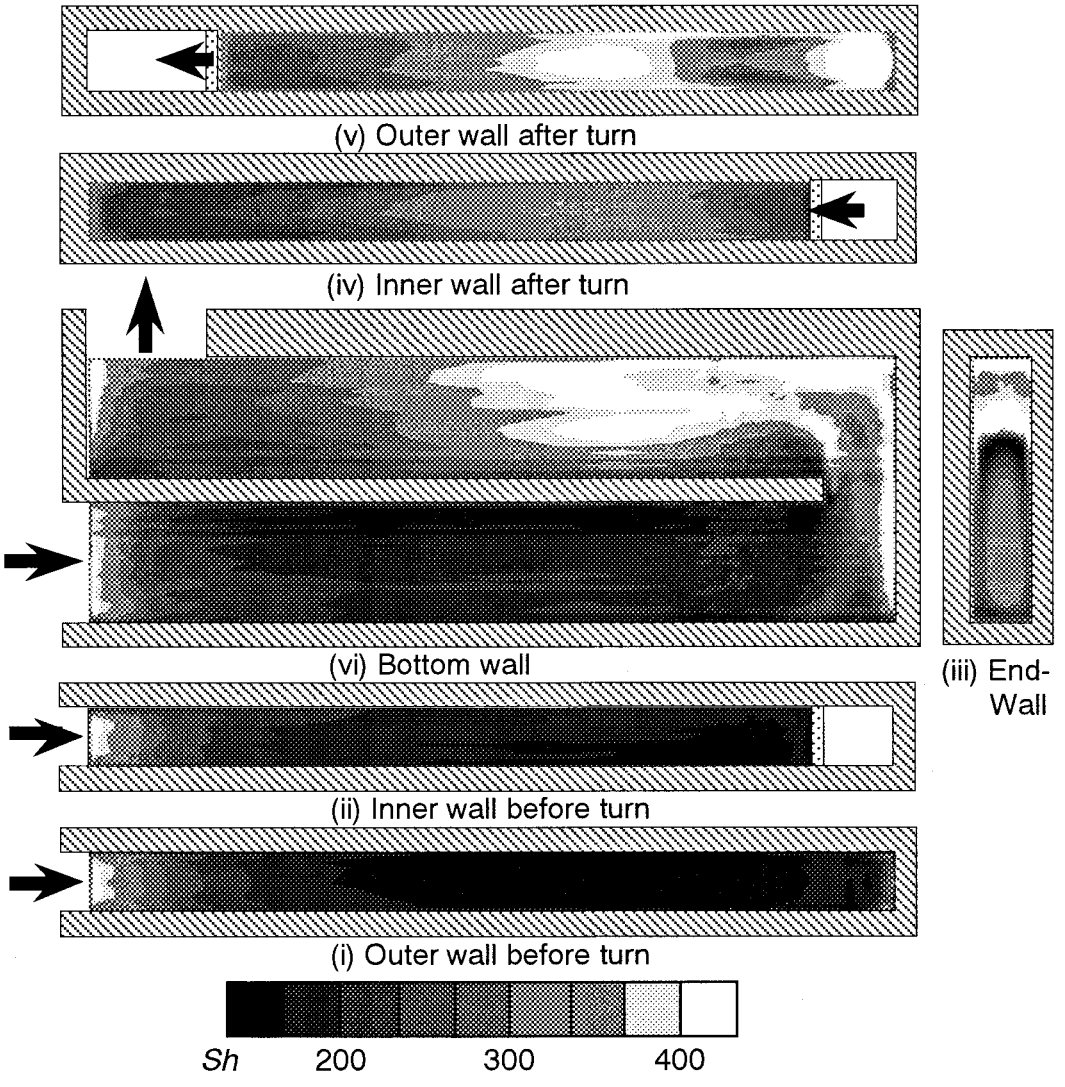

Fig. 14. Local Sherwood number distribution ($C = 30$ mm, $Re = 3.5 \times 10^4$).

3.5.3. Straight section after the turn

Since the flow exiting the turn section is separated at the tip of the inner wall, a separation bubble is formed along the inner wall after the turn [1]. The mass transfer is deteriorated in this separation bubble due to the recirculation of the flow, and thus *Sh* on the inner wall (Fig. 13(iv)) and on the bottom wall reaches its local minimums near the tip of the inner wall. On the other hand, in Block 9 on the outer wall (Fig. 13(v)), the region of relatively high *Sh*-values still remains near the spanwise centerline of the wall after the local maximum in Block 8.

In Block 10, *Sh* attains its local maximum on all channel walls, corresponding to the local maximums of Sh_B in Fig. 11. It is thought that such large mass transfer rates in Block 10 are caused by the reattachment of the flow which is separated at the inner-wall tip [1,10]. On the bottom wall, the region of high *Sh*-values occupies most of Block 10, and no spanwise deviations are observed clearly in the *Sh* distribution. On the other hand, on the short-side walls, *Sh*-values on the inner wall are larger than those on the outer wall if compared at the same streamwise location in Block 10. It is thought that the flow separated at the inner-wall tip is unsteady, and that the location of the flow reattachment can change over time. From the *Sh* distributions on the short-side walls shown here, it follows that under the present experimental condition the separated flow reattaches on the inner wall, in Block 10, in the sense of time-mean location averaged during the period of data run.

After Block 11, *Sh* decreases gradually as the flow

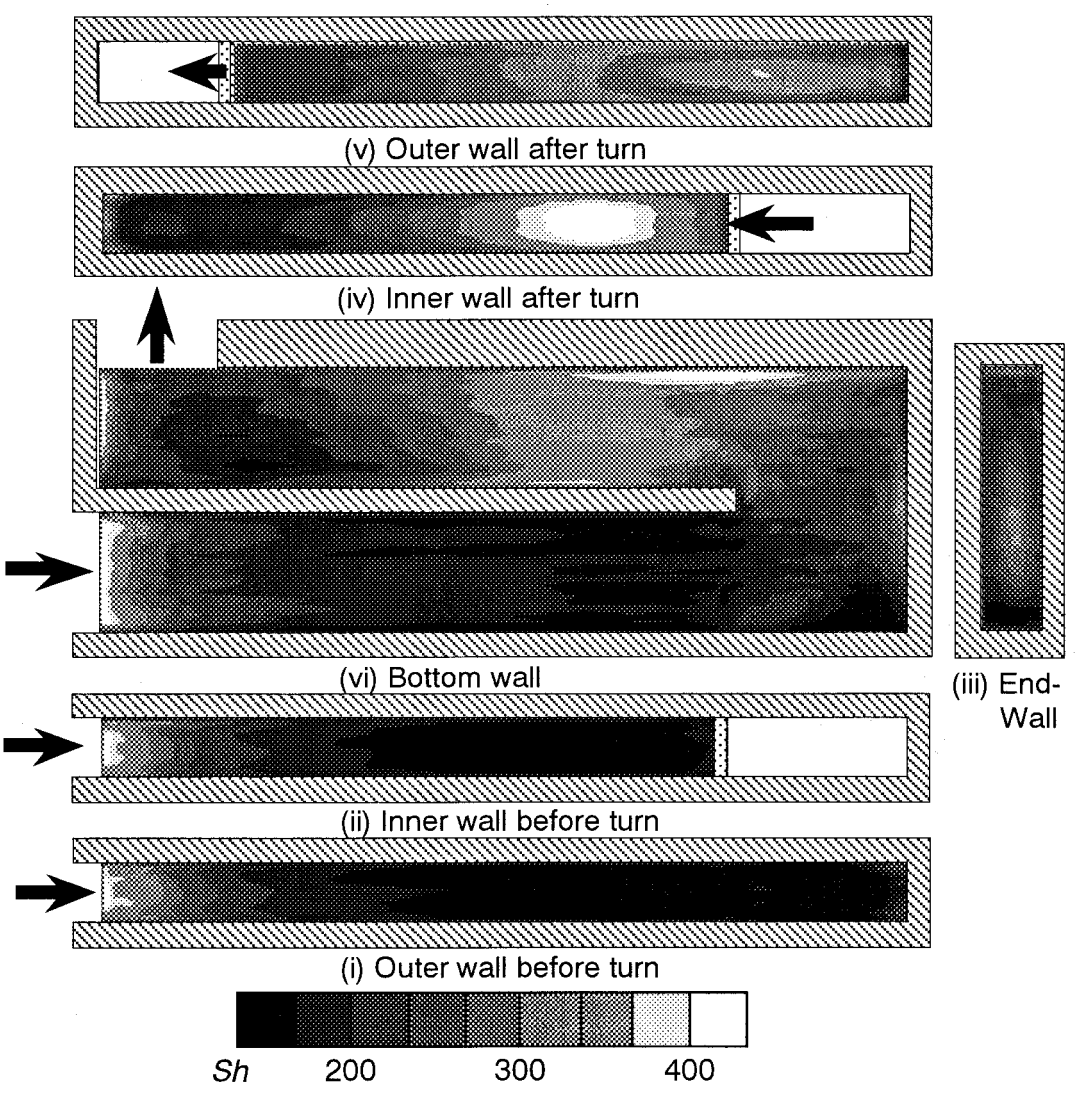

Fig. 15. Local Sherwood number distribution ($C = 70$ mm, $Re = 3.5 \times 10^4$).

proceeds downstream. A detailed comparison of *Sh* distributions obtained at an equal streamwise location reveals that the values of *Sh* in the outer-wall side are larger than those in the inner-wall side. This spanwise non-uniformity of *Sh* distribution suggests that the flow field after the turn section has a deflection in the primary flow with higher velocity toward the outer wall.

3.6. Influence of turn clearance on local Sherwood number

Fig. 14 shows the *Sh* distributions obtained in the channel with a narrower turn clearance of $C = 30$ mm for $Re = 3.5 \times 10^4$. In the upstream half of the turn section, the region of high *Sh*-values occupies a rather large area on the bottom wall near the junction with the end wall, and the recirculation zone of low *Sh*, such as observed in the corner of Fig. 13(vi), almost disappears. These results show that the influence of decreasing C on the *Sh* distribution appears in the regions not only in the downstream regions but also upstream of the turn clearance.

In the downstream half of the turn section, the mass transfer is much enhanced on all walls because the flow impinging on the outer wall is accelerated by reducing the turn clearance and, as a result, the flows blowing down on the bottom wall and reversed to the end wall after impinging on the outer wall have higher velocities. Near the streamwise midpoint of the end

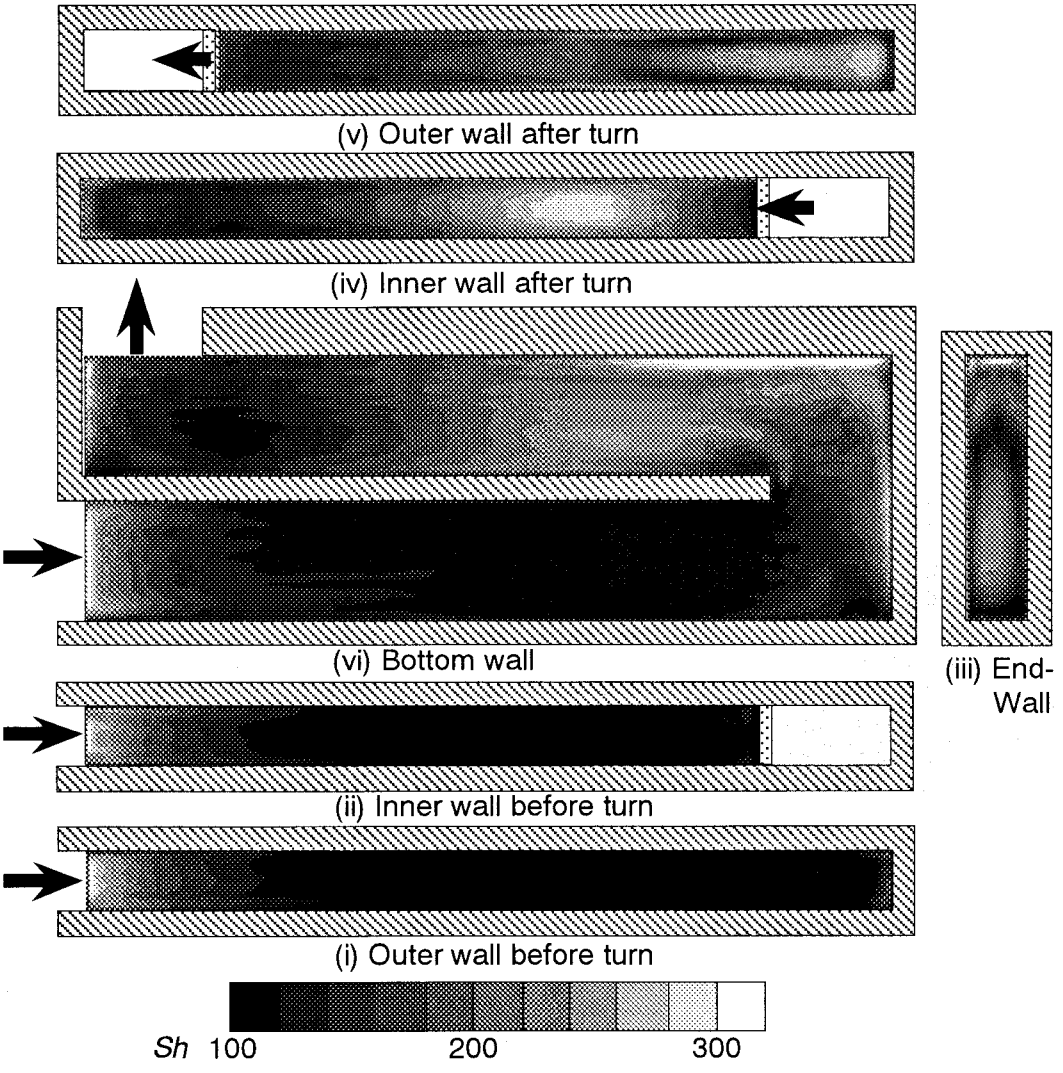

Fig. 16. Local Sherwood number distribution ($C=50$ mm, $Re=2.0\times10^4$).

wall, however, *Sh* reaches its local minimum as in the case of $C=50$ mm, and its value is almost the same as that shown in Fig. 13(iii).

In the straight section after the turn, the values of *Sh* are much larger than those in Fig. 13 to the exit of the test section; this suggests that the effect of reducing the turn clearance on *Sh* is maintained down to the region located far from the turn section. As in the case of $C=50$ mm, the low mass transfer region corresponding to the separation bubble is formed along the inner wall near its tip, and *Sh* attains the local maximum in Block 10. The local mass transfer characteristics in and after Block 10 are, however, remarkably different from those for $C=50$ mm. In Fig. 13(iv) and 13(v), *Sh*-values in Block 10 on the inner wall were larger than those on the outer wall, and thus it was estimated that the flow which separated at the inner-wall tip reattaches on the inner wall. In contrast, in Block 10 of the present channel with $C=30$ mm, the local maximum of *Sh* on the outer wall is larger than that on the inner wall. This means that, as opposite to the case of $C=50$ mm, the flow which separated at the inner-wall tip reattaches on the outer wall in the present channel. After the flow attachment, the deflection of the high *Sh* region to the outer-wall side is also observed to be similar to the case of $C=50$ mm, but the spanwise non-uniformity of *Sh* distribution observed in Fig. 14(vi) is more pronounced than that in Fig. 13(vi).

Fig. 15 shows the *Sh* map obtained for the largest turn clearance of 70 mm. In the upstream (first) corner of the turn section, the region of low *Sh*-values corre-

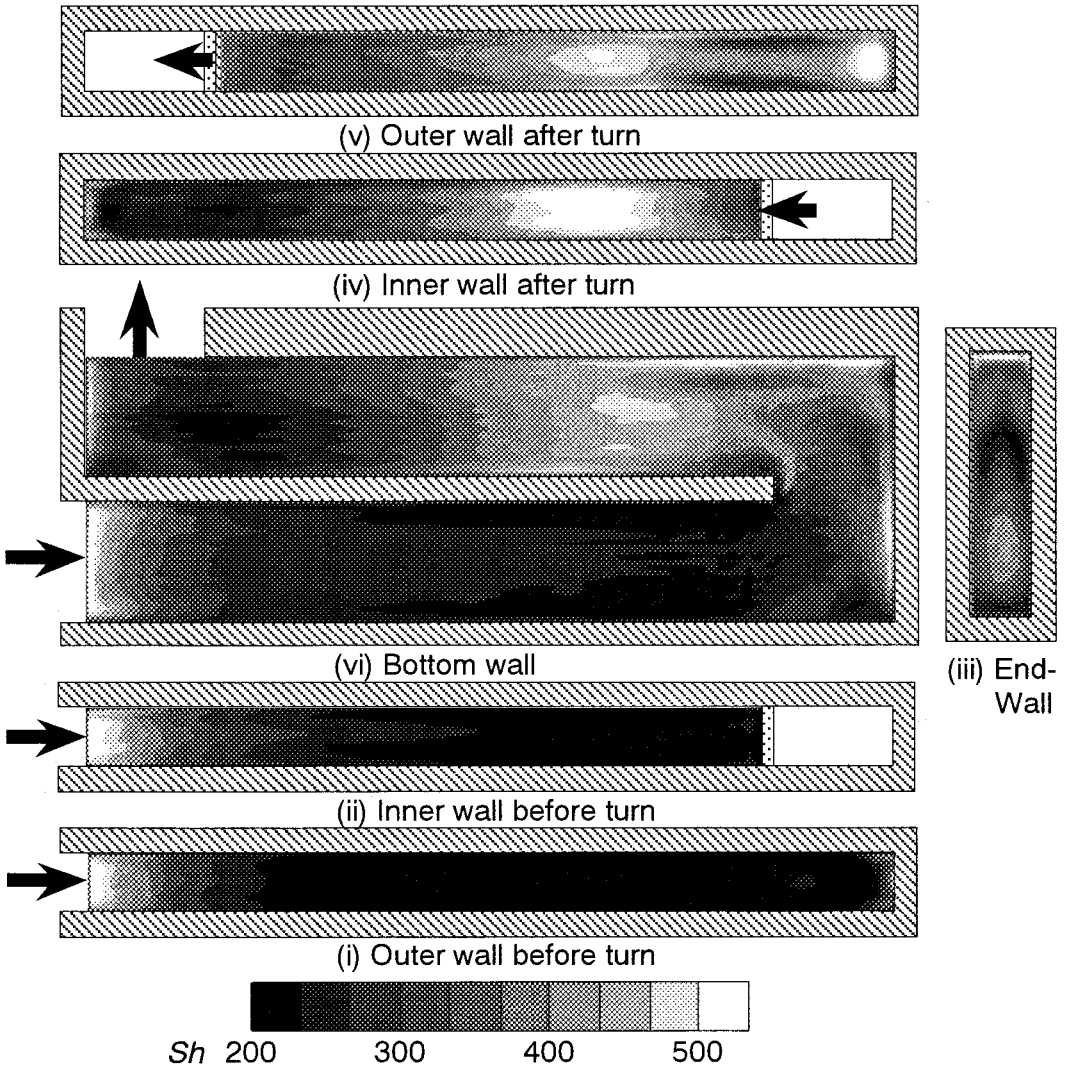

Fig. 17. Local Sherwood number distribution ($C = 50$ mm, $Re = 5.0 \times 10^4$).

sponding to the recirculation zone occupies a larger area on the bottom and end walls than that for the smaller turn clearances. On the end wall, *Sh* shows the local maximum in Block 7e as similar to the other channels, but the second local maximum that was observed in Block 8e of Figs. 13(iii) and 14(iii) does not appear so clearly in Fig. 15(iii); it can be observed in a very narrow region immediately next to the downstream (second) corner. Moreover, in Block 8 on the outer wall, *Sh* is not as high as that in the other channels.

Downstream of the separation bubble that exists along the inner wall after the turn, *Sh* attains its local maximum in Block 10 similar to Figs. 13 and 14. In Block 10, the values of *Sh* on the inner wall are much larger than those on the outer wall, suggesting that the flow which separated at the inner-wall tip reattaches on the inner wall as in the case of $C = 50$ mm. Moreover, a detailed comparison of Figs. 13–15 reveals that the local maximum of *Sh* on the short-side wall after the separation bubble appears around the center of Block 10 irrespective of the difference in the turn clearance. This means that the streamwise distance from the flow separation, i.e., inner-wall tip, to the flow reattachment becomes shorter as the turn clearance is increased.

3.7. Influence of Reynolds number on local Sherwood number

Fig. 16 shows the *Sh* distributions obtained in the same channel as Fig. 13 ($C = 50$ mm) under a smaller

Reynolds number of 2.0×10^4, and Fig. 17 shows those for a larger Re of 5.0×10^4. In the straight section before the turn and in the turn section, the Sh distributions on all channel walls of Figs. 13, 16, and 17 agree qualitatively well with one another. After the turn section, however, the influence of the Reynolds number on the Sh-distribution can be described as follows.

Under a lower Re, Sh on the inner wall shown in Fig. 16(iv) attains its local maximum in Block 10 after the separation bubble in Block 9; whereas on the outer wall of Fig. 16 (v), the values of Sh in Block 10 are not as large as those on the inner wall. Such characteristics of Sh distribution are similar to those observed in Fig. 13 (iv) and (v) for $Re = 3.5 \times 10^4$. On the other hand, in Block 10 of Fig. 17 for a larger Re, the difference between the Sh-values on the inner and outer walls is not so large as that observed in Block 10 of Figs. 13 and 16.

A similar trend as described here was also observed in the channel of $C = 70$ mm. In the case of $C = 30$ mm, however, the values of Sh in Block 10 on the outer wall were much larger than those on the inner wall under any Re tested here, and the qualitative characteristics of Sh distribution were independent of the Reynolds number. From these results, Re-dependency of the flow field in the present channels can be estimated as follows. In the channel with a relatively large turn clearance, the flow which separated at the inner-wall tip mostly reattaches on the inner wall under a low Re condition; as Re is increased, however, the unsteadiness of the flow after the turn is intensified, and this separated flow tends to occasionally reattach on the outer wall as well as on the inner wall. On the other hand, in the channel with a small turn clearance, the unsteadiness of the flow reattachment is weaker than in the case of a larger turn clearance, and the flow field after the turn is somewhat insensitive to the Reynolds number.

4. Conclusions

1. In all channels tested in this study, the mean Sherwood number Sh_m increases exponentially with the Reynolds number, and the Sherwood number averaged in the downstream half of the test section is 1.3–1.4 times as large as that of the upstream half. The values of Sh_m for $C = 70$ mm are almost the same as those for $C = 50$ mm, whereas Sh_m for $C = 30$ mm is 1.3 times as large as that for $C = 50$ mm.
2. The global distributions of the block-averaged Sherwood number Sh_B on the long-side wall are quite similar to those on the short-side walls, and the maximum Sh_B is observed in Block 10 a few d_h downstream of the inner-wall tip irrespective of the turn clearance. On the outer wall and bottom wall, Sh_B-values for $C = 30$ mm are larger than those for other channels in and after the turn section. On the inner wall, however, the influence of C on Sh_B does not appear as clearly as on the other walls.
3. In the turn section, the local Sherwood number Sh becomes much larger than that in the straight section before the turn, but the recirculation zone of low Sh-values appears in the upstream (first) corner of the turn. On the end wall, there appear two local maximums of Sh; the first one is observed in the upstream half of the wall, and the second one appears near the downstream edge of the wall. In the channel of $C = 70$ mm, however, the latter appears in a very narrow region near the downstream (second) corner and is not so clear as that in the other channels. Sh also attains its local maximum on the outer wall in the downstream half of the turn section due to the flow that impinges against this wall after passing through the turn clearance.
4. In the straight section after the turn, the flow which is separated at the inner-wall tip forms a separation bubble along the inner wall, and low Sh regions corresponding to it appear on the bottom and inner walls. In the channels of $C = 50$ and 70 mm under a relatively low Re, this separated flow reattaches on the inner wall (in Block 10) where Sh attains its local maximum. As Re is increased, however, the local maximums of Sh tend to appear not only on the inner wall but also the outer wall. In the channel of $C = 30$ mm, the separated flow reattaches on the outer wall irrespective of Re. In all channels tested here, Sh in the outer-wall side shows larger values than that in the inner-wall side in the region after the flow reattachment.

Acknowledgements

The authors express their thanks to Mr N. Shiraki and Mr K Tachibana, Research Engineers in the School of Engineering of Nagoya University, for their assistance in producing the experimental apparatus. They also wish to thank Mr M Yanagida, postgraduate student of Nagoya University, for his assistance in conducting the experiment.

References

[1] D.E. Metzger, C.W. Plevich, C.S. Fan, Pressure loss through sharp 180-deg turns in smooth rectangular

channels, Journal of Engineering for Gas Turbines and Power 106 (1984) 677–681.
[2] D.E. Metzger, M.K. Sahm, Heat transfer around sharp 180-deg turns in smooth rectangular channels, Journal of Heat Transfer 108 (1986) 500–506.
[3] C.S. Fan, D.E. Metzger Effects of channel aspect ratio on heat transfer in rectangular passage sharp 180-deg turns. ASME Paper, 87-GT-113 (1987).
[4] M.K. Chyu, Regional heat transfer in two-pass and three-pass passages with 180-deg sharp turn, Journal of Heat Transfer 113 (1991) 63–70.
[5] J.H. Wagner, B.V. Johnson, F.C. Kopper, Heat transfer in rotating serpentine passages with smooth walls, Journal of Turbomachinery 113 (1991) 321–330.
[6] W.J. Yang, N. Zhang, J. Chiou, Local heat transfer in a rotating serpentine flow passage, Journal of Heat Transfer 114 (1992) 354–361.
[7] S. Mochizuki, J. Takamura, S. Yamawaki, W.J. Yang, Heat transfer in serpentine flow passages with rotation, Journal of Turbomachinery 116 (1994) 133–140.
[8] S. Dutta, J.C. Han, Local heat transfer in rotating smooth and ribbed two-pass square channels with three channel orientations, Journal of Heat Transfer 118 (1996) 578–584.
[9] D.L. Besserman, S. Tanrikut, Comparison of heat transfer measurements with computations for turbulent flow around a 180-deg bend, Journal of Turbomachinery 114 (1992) 865–871.
[10] T.S. Wang, M.K. Chyu, Heat convection in a 180-deg turning duct with different turn configurations, Journal of Thermophysics and Heat Transfer 8 (1994) 595–601.
[11] T. Astarita, G. Cardone, G.M. Carlomagno, Heat transfer and surface flow visualization around a 180-deg turn in a rectangular channel, Heat Transfer in Turbulent Flows, ASME HTD- 318 (1995) 161–168.
[12] M. Hirota, H. Fujita, A. Tanaka, S. Araki, T. Tanaka, Local heat (mass) transfer characteristics in rectangular ducts with a sharp 180-deg turn, Energy Conversion and Management 38 (1997) 1155–1168.
[13] J.C. Han, P.R. Chandra, S.C. Lau, Local heat/mass transfer distributions around sharp 180 deg turns in two-pass smooth and rib-roughened channels, Journal of Heat Transfer 110 (1988) 91–98.
[14] P.R. Chandra, S.C. Lau, J.C. Han, Effect of rib angle on local heat/mass transfer distribution in a two-pass rib-roughened channel, Journal of Turbomachinery 110 (1988) 233–241.
[15] A. Murata, S. Mochizuki, M. Fukunaga, Detailed measurement of local heat transfer in a square-cross-sectioned duct with a sharp 180-deg turn, in: Proceedings of the Tenth International Heat Transfer Conference, 4, Taylor and Francis, 1994, pp. 291–296.
[16] J.P. Johnston, Internal Flow, in: P. Bradshaw (Ed.), Turbulence, Springer-Verlag, Berlin, 1976 (Chap. 3).
[17] S.M. Chang, J.A.C. Humphrey, A. Modavi, Turbulent flow in a strongly curved U-bend and downstream tangent of square cross-sections, Physico Chemical Hydrodynamics 4 (1983) 243–269.
[18] R.W. Johnson, B.E. Launder, Local Nusselt number and temperature field in turbulent flow through a heated square sectioned U-bend, International Journal of Heat and Fluid Flow 6 (1985) 171–180.
[19] R.W. Johnson, Numerical simulation of local Nusselt number for turbulent flow in a square duct with a 180° bend, Numerical Heat Transfer 13 (1988) 205–228.
[20] Y.D. Choi, H. Iacovides, B.E. Launder, Numerical computation of turbulent flow in a square-sectioned 180-deg bend, Journal of Fluids Engineering 111 (1989) 59–68.
[21] M. Breuer, W. Rodi, Large-eddy simulation of turbulent flow through a straight square duct and a 180° bend, in: P.R. Voke, L. Kleiser, J.P. Chollet (Eds.), Direct and Large-Eddy Simulation I, Kluwer Academic Publisher, Dordrecht, 1994, pp. 273–285.
[22] R.J. Goldstein, H.H. Cho, A review of mass transfer measurements using naphthalene sublimation, Experimental Thermal and Fluid Science 10 (1995) 416–434.
[23] E.M. Sparrow, N. Cur, Turbulent heat transfer in a symmetrically or asymmetrically heated flat rectangular duct with flow separation at inlet, Journal of Heat Transfer 104 (1982) 82–89.
[24] F. Burggraf, Experimental heat transfer and pressure drop with two-dimensional discrete turbulence promoters applied to two opposite walls of a square tube, in: E.E. Bergles, R.L. Webb (Eds.), Augmentation of Convective Heat and Mass Transfer, ASME, New York, 1970, pp. 70–79.